

# *Generation of Antimicrobial NO<sub>x</sub> by Atmospheric Air Transient Spark Discharge*

**M. Janda, V. Martišovitš, K. Hensel & Z. Machala**

**Plasma Chemistry and Plasma Processing**

ISSN 0272-4324

Plasma Chem Plasma Process  
DOI 10.1007/s11090-016-9694-5

Volume 35, Number 6  
November 2015

**ONLINE  
FIRST**

**Plasma  
Chemistry  
and Plasma  
Processing**

 Springer

 Springer

**Your article is protected by copyright and all rights are held exclusively by Springer Science +Business Media New York. This e-offprint is for personal use only and shall not be self-archived in electronic repositories. If you wish to self-archive your article, please use the accepted manuscript version for posting on your own website. You may further deposit the accepted manuscript version in any repository, provided it is only made publicly available 12 months after official publication or later and provided acknowledgement is given to the original source of publication and a link is inserted to the published article on Springer's website. The link must be accompanied by the following text: "The final publication is available at [link.springer.com](http://link.springer.com)".**

# Generation of Antimicrobial NO<sub>x</sub> by Atmospheric Air Transient Spark Discharge

M. Janda<sup>1</sup> · V. Martišovits<sup>1</sup> · K. Hensel<sup>1</sup> · Z. Machala<sup>1</sup>

Received: 7 July 2015 / Accepted: 10 January 2016  
© Springer Science+Business Media New York 2016

**Abstract** Atmospheric pressure air plasma discharges generate potential antimicrobial agents, such as nitrogen oxides and ozone. Generation of nitrogen oxides was studied in a DC-driven self-pulsing (1–10 kHz) transient spark (TS) discharge. The precursors of NO<sub>x</sub> production and the TS characteristics were studied by nanosecond time-resolved optical diagnostics: a photomultiplier module and a spectrometer coupled with fast intensified camera. Thanks to the short (~10–100 ns) high current (>1 A) spark current pulses, highly reactive non-equilibrium plasma is generated. Ozone was not detectable in the TS, probably due to higher gas temperature after the short spark current pulses, but the NO<sub>x</sub> production rate of  $\sim 7 \times 10^{16}$  molecules/J was achieved. The NO<sub>2</sub>/NO ratio decreased with increasing TS repetition frequency, which is related to the complex frequency-dependent discharge properties and thus changing NO<sub>2</sub>/NO generating mechanisms. Further optimization of NO<sub>2</sub> and NO production to improve the biomedical and antimicrobial effects is possible by modifying the electric circuit generating the TS discharge.

**Keywords** Non-equilibrium air plasma · Transient spark · Nitrogen oxides · Antimicrobial agents · Time-resolved optical diagnostic

## Introduction

Non-thermal (cold) plasmas generated by electrical discharges can be maintained at low gas temperatures, but have high electron energies responsible for their chemical activity. For this reason, several plasma based technologies were successfully implemented in the recent decades, in processes such as surface modification, flue gas cleaning, water purification,

---

✉ M. Janda  
janda@fmph.uniba.sk

<sup>1</sup> Division of Environmental Physics, Faculty of Mathematics, Physics and Informatics, Comenius University, Mlynská dolina F2, 84248 Bratislava, Slovakia

plasma assisted combustion, or hazardous liquid waste processing [1–4]. In the recent years, the plasma community witnesses a fast development of bio-medical applications [5, 6], since cold plasmas provide multiple agents that can efficiently kill bacteria and other hazardous microbes, and cause multiple biomedical and therapeutic effects in higher organisms [7–9].

In biomedical applications, the fundamental research to assess the roles of various plasma agents (e.g. UV radiation, electric field, reactive neutral and charged particles) involved is very important. At present, the major role in atmospheric pressure plasmas generated in air is typically attributed to reactive oxygen and nitrogen species (RONS) [10–13]. Plasmas in contact with water can simultaneously generate several aqueous RONS, such as nitrite  $\text{NO}_2^-$ , nitrate  $\text{NO}_3^-$ , peroxyxynitrite  $\text{ONOO}^-$ , dissolved ozone  $\text{O}_3$ , or hydrogen peroxide  $\text{H}_2\text{O}_2$  from the hydroxyl radicals OH. It is reasonable to assume that the overall bactericidal effect of the air plasma discharge involves synergistic effect of several of these species [12, 14].

The aqueous RONS are produced from the gaseous RONS, e.g. nitrogen oxides NO,  $\text{NO}_2$ , ozone  $\text{O}_3$  and OH radicals, generated by the plasma in gas and subsequently dissolved in water. Depending on the used electrical discharge, different gaseous RONS can dominate in the treated gas. For example, the  $\text{O}_3$  generation is very efficient by cold plasma sources, such as dielectric barrier or streamer corona discharges [15–17]. Water ozonation technology has been commercially used for more than a century. Various plasma sources can also generate significant amounts of  $\text{NO}_x$  [18–21]. The antibacterial potential of  $\text{NO}_2$  is known for a long time [22, 23], and has been already commercially introduced [24], but new types of discharges optimized for bio-medical plasma applications are still being developed and studied. Several recent papers report investigating the  $\text{NO}_x$  formation and their bactericidal effects in a hybrid glow-spark discharges or in dielectric barrier discharges in air [25–27].

In the present paper we focus on the synthesis of NO,  $\text{NO}_2$  and their precursors (O and N radicals) by the transient spark (TS) discharge in air. The TS is a DC-driven self-pulsing discharge with the repetition frequency 1–10 kHz. The TS is initiated by a streamer transforming to a short spark current pulse. Streamers are considered to be critical with respect to the efficiency of plasma induced chemistry at atmospheric pressure. The electric field in the streamer's head can reach more than 200 kV/cm [28, 29], so that the chemical and ionization processes are very efficient there. On the other hand, transition of streamers to spark or arc discharge [30, 31], often generating thermal plasma, is usually not desired in environmental and bio-medical applications. High power requirements limit the utilization of thermal plasmas usually only to applications where one can either expect valuable products, or needs to completely destroy dangerous pollutants [32–34].

The TS current pulses are sufficiently short ( $\sim 10$ – $100$  ns) to avoid the plasma thermalization. Non-equilibrium plasma generated during the spark phase of the TS is highly reactive, since the electron density as high as  $10^{17}$   $\text{cm}^{-3}$  can be achieved [35], and its chemical activity is comparable with nanosecond repetitively pulsed (NRP) spark discharges [36]. The advantage of TS is no need of special and expensive high voltage pulsers with high repetitive frequencies and nanosecond rise-times used to generate NRP discharges [37–39].

The TS has already been successfully tested for several environmental and bio-medical applications [11, 12, 40, 41], and extensive fundamental research of TS using several electrical and optical diagnostic methods has been performed [35, 42–46]. However, further research is needed for better understanding of chemical processes initiated by the TS. In this work we present research of TS using optical emission spectroscopy (OES)

combined with the post-discharge gas composition analysis, focused at the synthesis of NO, NO<sub>2</sub> and their precursors (O and N radicals).

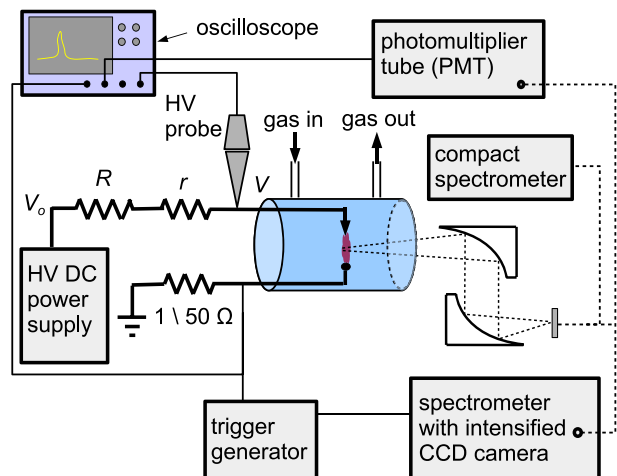
## Experimental Set-Up

DC high voltage (HV) power supply *Technix SR20-R-1200* (0–20 kV, 0–60 mA) connected to the anode via a series resistor ( $R = 4.92\text{--}9.84\text{ M}\Omega$ ) was used to generate a positive TS discharge between two stainless steel electrodes in point-to-point configuration with anode at the top. The distance  $d$  between the electrodes was varied between 4 and 6 mm. The electrodes were made of a 2-mm diameter rod. The anode tip was sharpened whereas the cathode was blunt. The curvature radius of the anode tip was of the order of 100  $\mu\text{m}$ . The curvature radius of the cathode was of the order of a millimeter. The electrodes were placed in a 10 cm long gas cell with the inner radius 4 cm and two valves for the gas inlet and outlet. One side of the glass tube was enclosed by Teflon window with openings for the electrodes. The other side was enclosed by the CaF<sub>2</sub> window enabling optical diagnostics. The schematic of the experimental set-up is depicted in Fig. 1.

The discharge voltage was measured by a HV probe *Tektronix P6015A* and the discharge current was measured on a 50 or 1  $\Omega$  resistor shunt. The 1  $\Omega$  resistor shunt was used to measure the spark current pulses; whereas the 50  $\Omega$  resistor shunt was used to measure the streamer current pulses. Electric signals were recorded by a 200 MHz digitizing oscilloscope *Tektronix TDS2024* (200 MHz, sampling rate up to 2 Gs/s). The mean discharge current  $I_{mean}$  was estimated from the current  $I_o$  delivered and directly measured by the DC power supply, taking into account losses due to the parasitic current through the HV probe.

The experiments were carried out in synthetic air driven from the pressure tanks (N<sub>2</sub>:O<sub>2</sub> = 4:1, N<sub>2</sub>: 99.99 % purity, O<sub>2</sub>: 99.5 % purity), with a flow rate 1.3–2.6 l min<sup>-1</sup>. A gas analyzer *Kane KM9106 Quintox* was used to measure the gas composition after passing through the discharge reactor. It detects NO and NO<sub>2</sub> in the range of 0–5000 ppm, or 0–1000 ppm, respectively, with an accuracy of  $\pm 5$  ppm (<100 ppm), or  $\pm 5$  % (>100 ppm). In addition, Fourier transform infrared (FT-IR) spectrophotometer *Shimadzu*

**Fig. 1** Simplified schematic of the experimental set-up



*IRAffinity-1S* (wavenumber range 7800–350  $\text{cm}^{-1}$ , best spectral resolution 0.5  $\text{cm}^{-1}$ ) was used for the detection of  $\text{O}_3$  and other nitrogen oxides, such as  $\text{N}_2\text{O}$  or  $\text{N}_2\text{O}_5$ . We also used the FT-IR spectrophotometer to verify the *Kane* gas analyzer measurement of the nitrogen oxides density in the treated post-discharge gas.

For fast recording of time-integrated broadband emission spectra (200–1100 nm), we used a dual-channel fiber optic compact emission spectrometer *Ocean Optics SD2000* (spectral resolution 0.6–1.7 nm). The time-resolved emission spectra were obtained using a 2 m monochromator *Carl Zeiss Jena PGS2* (spectral resolution 0.04–0.09 nm), covering the UV and VIS regions (200–800 nm), coupled with an intensified charge-coupled device (iCCD) camera *Andor Istar* (minimum gate 2 ns). The light collection was provided by a pair of parabolic mirrors focused on a small area near the anode tip. These mirrors, together with the optical fiber core diameter, determined the spatial resolution of 300  $\mu\text{m}$ .

The iCCD camera was triggered by a 5 V rectangular pulse generator with  $<5$  ns rise time. This generator was triggered directly by the discharge current signal, causing an additional delay of  $<10$  ns. This delay, plus the delay caused by the transmission of the signal by BNC cables, was compensated by using a 10 m long optical fiber *Ocean Optics P400-10-UV-VIS*. For measurements with the iCCD camera, an additional small resistor  $r = 1$  k $\Omega$  was attached directly to the anode. The purpose of additional  $r$  was to eliminate the current signal oscillations induced by the internal inductances of the grounding wire and the HV cable connecting  $R$  with the anode that caused problems with the iCCD camera triggering. More details about the role of  $r$  on the characteristics of the TS discharge can be found in Ref. [43].

For fast measurements of the emission intensity evolution, we used a photomultiplier tube (PMT) module *Hamamatsu H955* (rise time 2.2 ns). In order to isolate a specific spectral transition for PMT measurements, a bandpass interference filter, e.g. *Melles Griot 03 FIU127* for the  $\text{N}_2$  (C–B, 0–0) transition, was inserted into the optical path. The PMT module signal was recorded using the oscilloscope.

## Results and Discussion

### Discharge Properties

Transient spark is initiated by a streamer, when the potential on the stressed electrode  $V$  reaches voltage  $V_{TS}$ , characteristic for the TS (corresponding time  $\approx -500$  ns in Fig. 2). The streamer forms a relatively conductive plasma channel between the electrodes. This leads to partial discharging of the electric circuit internal capacitance  $C$ . The current from the partial discharging of  $C$  heats up the gas inside the plasma channel generated by the streamer. The transition to spark occurs when gas temperature inside the plasma channel increases to  $\sim 1000$  K [44].

During the spark phase, the electric circuit internal capacitance discharges completely, the voltage on the HV electrode drops to almost zero (time 0 ns in Fig. 2), and the discharge current given approximately by

$$I \approx -C \times \frac{dV(t)}{dt}, \quad (1)$$

reaches a high value ( $\sim 1$ –10 A). Transition to an arc after the spark phase is restricted by the large ballast resistor  $R$ . It limits the DC current delivered to the plasma after  $C$  is discharged. For  $R \approx 10$  M $\Omega$ , even for maximum possible applied voltage 20 kV, the DC

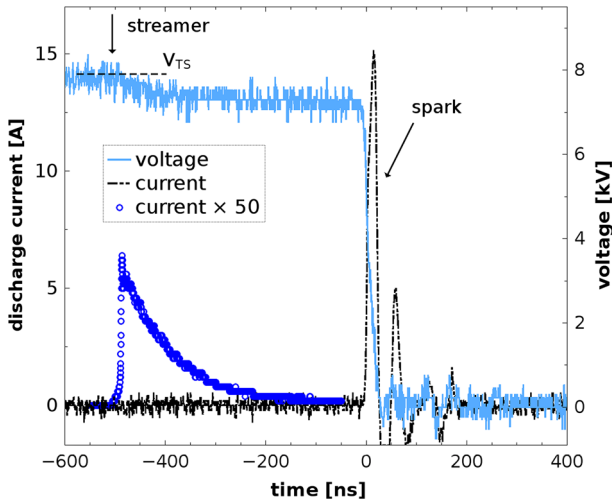


**Fig. 2** Typical transient spark voltage and current waveforms,  $d \approx 6$  mm,  $C \approx 35$  pF,  $R = 9.24$  M $\Omega$ ,  $f \approx 2$  kHz,  $r = 0$  k $\Omega$ . Streamer current waveform (blue circles) was measured on 50  $\Omega$  shunt, while the current waveform showing spark pulse (black dashed line) was measured on 1  $\Omega$  shunt (Color figure online)

current is certainly below 2 mA: not high enough to maintain DC discharge after the TS spark phase. As a result, the plasma decays after the spark pulse. Eventually, the plasma resistance exceeds the  $R$  and the potential  $V$  on the anode gradually increases, as the capacitance  $C$  recharges. A new TS pulse, initiated by a new streamer, occurs when the potential  $V$  reaches the breakdown voltage  $V_{TS}$  again. The TS is thus based on repetitive charging and discharging of  $C$ . The repetition frequency  $f$  of this process can be controlled by the DC power supply voltage  $V_o$  and is typically in the range 1–10 kHz [43].

The TS repetition frequency increase is accompanied by the increase of the mean discharge current  $I_{mean}$  and discharge power  $P$  (Fig. 3), estimated as

$$P \approx f \times E_p. \tag{2}$$

Here,  $E_p$  is the energy delivered to the gap per pulse. The  $E_p$  can be estimated using two different formulas:

$$E_p \approx \frac{1}{2} CV_{TS}^2 \approx \int_{\tau} V(t) \times I(t) dt, \tag{3}$$

where the time interval  $\tau$  is chosen so that voltage and current waveforms cover the whole active phase of TS discharge, from beginning of the streamer to the end of the spark (Fig. 2). Both approaches were tested to determine the  $E_p$  and the difference between the results was within their uncertainties. We further used the first approach because of its simplicity. The capacitance  $C$  was estimated from the measured current and voltage waveforms using Eq. (1).

Besides  $I_{mean}$  and  $P$ , several other TS discharge characteristics change with frequency as well [43, 44]. The breakdown voltage  $V_{TS}$  decreases, and the spark pulses are getting broader and smaller. Due to decrease of  $V_{TS}$ , the energy delivered to the gap per pulse  $E_p$

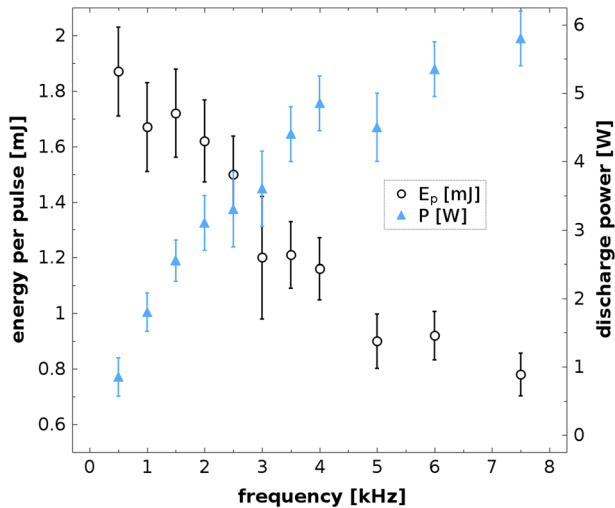


**Fig. 3** The discharge power  $P$  and energy per pulse  $E_p$  as functions of TS repetition frequency,  $d \approx 6$  mm,  $C \approx 35$  pF,  $R = 9.24$  M $\Omega$ ,  $r = 0$  k $\Omega$

decreases also with the increasing TS repetition frequency (Fig. 3), as can be deduced from Eq. (3).

The analysis of the electric circuit representing the TS, and the measurement of the discharge channel diameter by the time-resolved imaging enabled us to estimate the electron density  $n_e$  in TS from the current and voltage waveforms [35, 43]. After the streamer,  $n_e \approx 10^{14}$  cm $^{-3}$  was obtained, which is in an agreement with values found in the literature [28, 47–49]. During the spark phase, the electron density as high as  $10^{17}$  cm $^{-3}$  can be achieved at  $f < 4$  kHz. Generated plasma is thus strongly ionized for a short time. However, the TS spark current pulses are sufficiently short to avoid thermalization of generated plasma. With increasing TS repetition frequency, smaller and broader spark current pulses occur and the peak electron density decreases to  $\sim 10^{16}$  cm $^{-3}$  [35].

The time-integrated emission spectroscopy study confirmed that TS pulses generate highly reactive non-equilibrium plasma with excited atomic radicals ( $O^*$ ,  $N^*$ ), excited molecules  $N_2^*$  and ions  $N_2^{+*}$  (Fig. 4). The rotational temperature  $T_r$ , derived from the  $N_2$  2nd positive system of the time-integrated spectra, ranging from 500 to 1500 K depending on  $f$ , is much lower than the vibrational temperature (3800–5000 K). The TS emission characteristics change with increasing frequency as well. Below  $\sim 3$  kHz, atomic lines emission ( $O^*$ ,  $N^*$ ) and molecular  $N_2$  2nd positive system dominates in the spectra. The absolute intensities of  $N_2$  2nd and 1st positive systems per single TS pulse do not change significantly with the increasing frequency, but the intensities of atomic lines emission weaken with increasing  $f$  (Fig. 4). This might be interpreted as a decrease of the TS ability to produce radicals at higher frequencies, and the measurement of the generated  $NO_x$  density should reflect it as well.

### Nitrogen Oxides Generation Efficiency

The density of both  $NO$  and  $NO_2$  increase with  $f$  (Fig. 5) due to increasing discharge power  $P$ . However, the rate of this increase weakens as the frequency grows. This is related to the

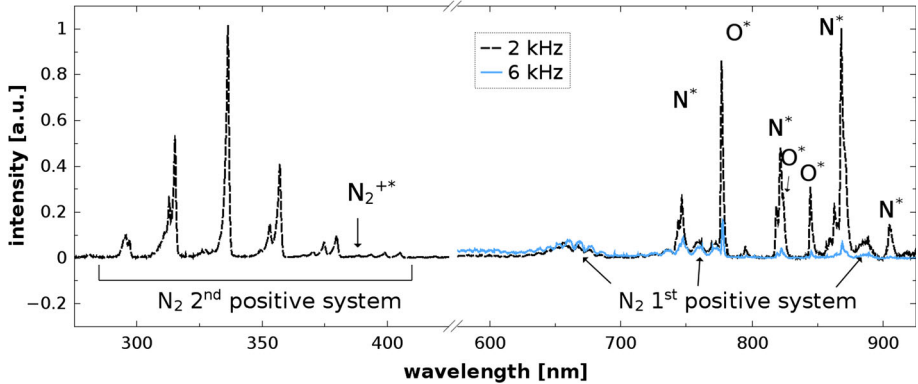


**Fig. 4** Typical time-integrated spectra of the TS discharge in air at repetition frequencies 2 and 6 kHz. In the UV range, the differences between 2 and 6 kHz were small, resulting only from different rotational and vibrational temperature of  $N_2(C)$  species. Thus, the spectrum at 6 kHz is not displayed for clarity. In the VIS range, the spectrum at 2 kHz is normalized to unity, while the spectrum at 6 kHz is normalized by the same factor multiplied by three, taking into account three times higher number of pulses per unit time at 6 kHz than at 2 kHz

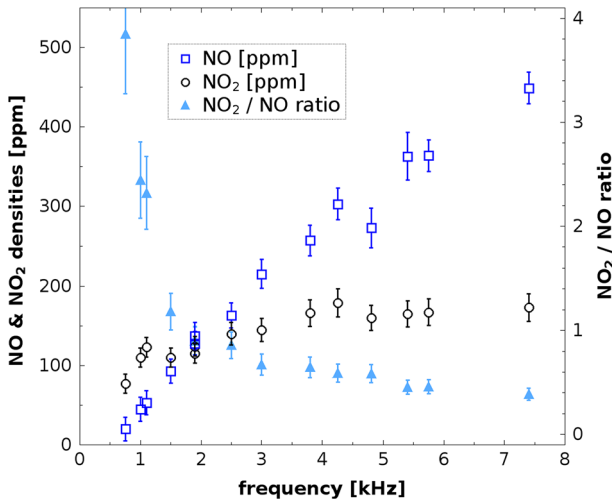


**Fig. 5** The NO and  $NO_2$  densities and their ratio as functions of TS repetition frequency,  $d \approx 6$  mm,  $C \approx 35$  pF,  $R = 9.24$  M $\Omega$ ,  $r = 0$  k $\Omega$ , synthetic air flow rate  $1.7$  l  $min^{-1}$

logarithmic-like dependence of  $P$  on  $f$ , resulting from the decrease of  $E_p$  with increasing frequency (Fig. 3). In order to assess the NO and  $NO_2$  generation efficiency at different TS frequency, it is thus necessary to take into account the changes of the input energy density. Other nitrogen oxides can be neglected in the first approximation, due to their absence in the measured infrared spectra.

Figure 6 shows the generation rate of NO and  $NO_2$  as number of molecules generated per input energy 1 J. The highest  $NO_x$  (NO +  $NO_2$ ) generation rate achieved is around  $7 \times 10^{16}$  molecules/J. This is higher than in the work of Pavlovich et al. [25], where

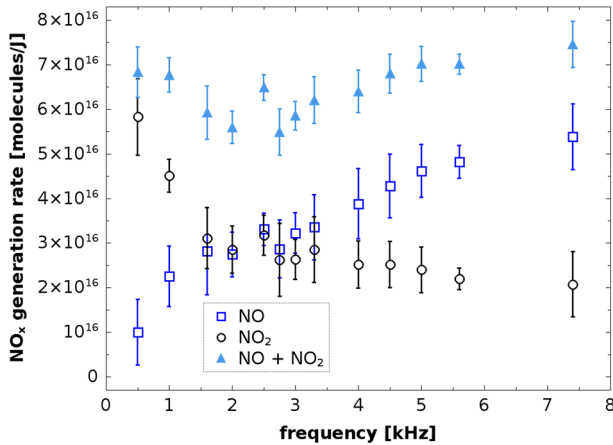


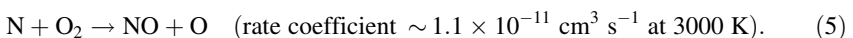
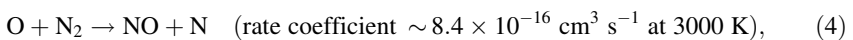
**Fig. 6** The NO and NO<sub>2</sub> generation rate (molecules/J) as function of TS repetition frequency,  $d \approx 6$  mm,  $C \approx 35$  pF,  $R = 9.24$  M $\Omega$ ,  $r = 0$  k $\Omega$ , averaged for flow rates 1.3–2.6 l min<sup>-1</sup>

similar type of a discharge was used (initial production rate  $1.5 \times 10^{16}$  molecules/J). On the other hand, higher generation rates were obtained using different types of discharges ([20] and references therein). For example, NO<sub>x</sub> production rate as high as  $(10\text{--}40) \times 10^{16}$  molecules/J was reached in an arc discharge [50]. We assume that we can still improve NO<sub>x</sub> generation efficiency our system by varying parameters of the electric circuit generating the TS discharge (external resistor, internal capacitance, distance of electrodes). Moreover, the NO<sub>x</sub> generation rate in the gas phase is not the only parameter to be considered for water bio-decontamination application. Here, the NO<sub>x</sub> transfer from the gas to the liquid phase can be a limiting step. From this point of view, the TS represents a promising alternative, as it can operate in direct contact with the treated water [41]. With water being supplied via a hollow anode [12, 41], the TS can even induce electrospray of the treated water and the gas–liquid interaction area enhancement to facilitate the mass transfer towards bacteria or cells suspended in water solutions.

The NO<sub>x</sub> generation rate can be also used to evaluate the TS ability to induce chemical changes with increasing repetition frequency. The NO generation rate tends to improve with increasing  $f$ , while the NO<sub>2</sub> generation rate decreases. As a result, the total NO<sub>x</sub> generation rate does not change significantly and does not support the hypothesis of weaker chemical reactivity of TS at higher frequencies. It seems it is rather the NO<sub>x</sub> synthesis mechanism that changes with  $f$ , leading either preferentially to NO or to NO<sub>2</sub> generation.

### Nitrogen Oxides Generation Mechanism

Despite the fact that TS generates ‘cold’ non-equilibrium plasma, the temperature during the spark phase of the TS can be as high as  $\sim 3000$  K ( $T_{spark}$ , Fig. 7). We therefore have to consider the Zeldovich thermal mechanism of the NO<sub>x</sub> generation. This mechanism is initiated by the thermal decomposition of N<sub>2</sub> and O<sub>2</sub> into their atomic states at high temperature (above  $\sim 1500$  K). Next, both N and O atomic radicals are able to produce NO:



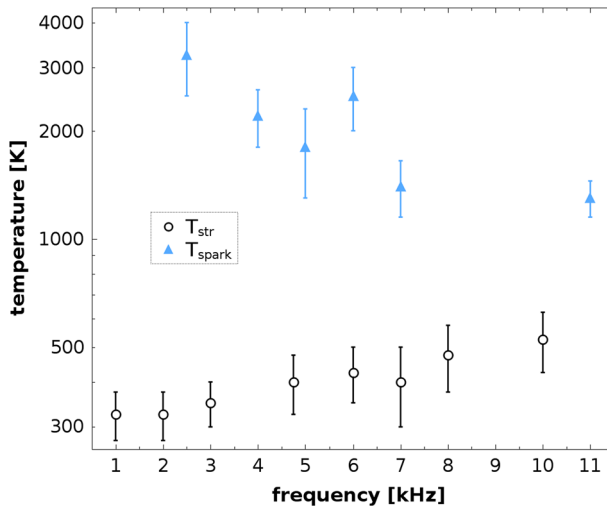


**Fig. 7** Temperature at the beginning of the streamer phase and the highest temperature during the spark phase of the TS as functions of  $f$ ,  $d \approx 5$  mm,  $C \approx 32$  pF,  $R = 9.84$  M $\Omega$ ,  $r = 1$  k $\Omega$

The rate coefficient of the second reaction with N atoms is four orders of magnitude higher at 3000 K, but production of N atomic radicals via the thermal decomposition of  $N_2$  is very slow even at 3000 K (rate coefficient  $\sim 1.5 \times 10^{-24}$  cm<sup>3</sup> s<sup>-1</sup>) [51]. As a result, the thermal decomposition of  $N_2$  is rate-limiting step of the thermal NO formation. In non-thermal plasmas, alternative reaction pathways for the generation of N atomic radicals exist. Moreover, reactions (4) and (5) can be much faster if one of the reactants is in excited state [51, 52].

Another important fact is that the temperature necessary for the thermal NO generation remains high only for a certain time after the spark current pulse. Mixing with the ambient air between two successive TS pulses cools the gas between the electrodes down. The ‘steady-state’ gas temperature, at which the initiating streamer of the next TS event appears, starts only at about 350 K at  $f \approx 1$  kHz ( $T_{str}$ , Fig. 7). Unfortunately, we do not know exactly how long the temperature is high enough for the efficient thermal NO<sub>x</sub> formation after the spark phase of the TS discharge. We approximated  $T_{str}$  and  $T_{spark}$  by the rotational temperature  $T_r$  of the  $N_2(C)$  species, assuming that in atmospheric pressure air plasma  $T \approx T_r$ . The  $T_r$  was obtained by fitting the time-resolved (time window 5–20 ns) experimental emission spectra of the  $N_2$  2nd positive system (0–0 transition) with the simulated ones, using Specair program [53] (Fig. 8). This emission can be observed only for a short time (a few tens of ns) after the streamer and spark current pulses (see Figs. 9, 10, respectively). For this reason we cannot measure the entire temperature evolution between two successive TS pulses and thus we are not able to assess the role of the thermal Zeldovich mechanism on the overall NO<sub>x</sub> production precisely.

However, the  $T_{str}$  increases with TS repetition frequency up to  $\sim 600$  K at  $f \approx 10$  kHz, and this could theoretically accelerate the thermal NO<sub>x</sub> generation. On the other hand, the  $T_{spark}$  decreases with  $f$  and could be responsible for the opposite trend. In any case, we observed no significant effect of TS repetition frequency on the NO<sub>x</sub> generation rate (Fig. 6), and thus also no dependence on  $T_{str}$  or  $T_{spark}$ . We therefore assume that plasma

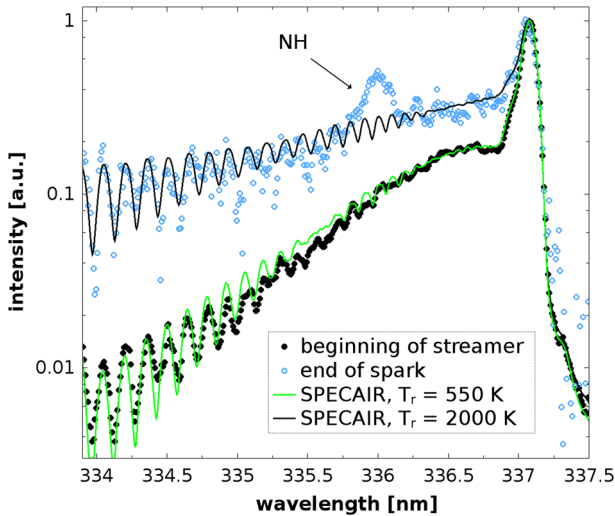


**Fig. 8** Experimental and Specair simulated spectra of  $N_2$  2nd positive system 0–0 transition,  $f \sim 5$  kHz, time resolution 20 ns,  $d \approx 5$  mm,  $C \approx 32$  pF,  $R = 9.84$  M $\Omega$ ,  $r = 1$  k $\Omega$

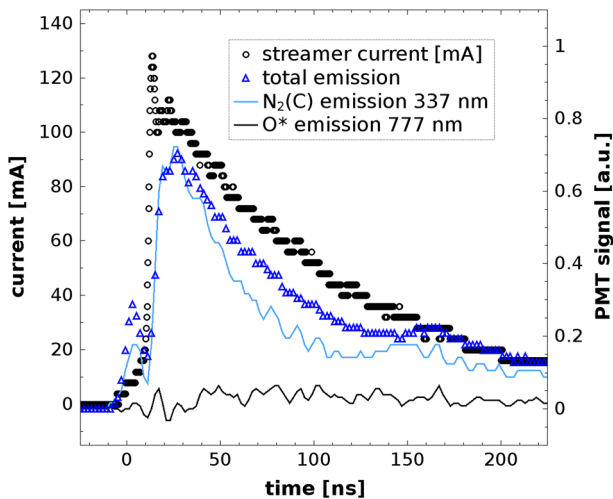


**Fig. 9** Typical PMT signals of the optical emission during the streamer phase of TS,  $f \sim 2$  kHz,  $d \approx 6$  mm,  $C \approx 35$  pF,  $R = 9.24$  M $\Omega$ ,  $r = 0$  k $\Omega$

processes, primarily initiated by high energy electrons, should play more important roles in the  $NO_x$  generation by the TS discharge than the Zeldovich thermal mechanism.

Information on the plasma processes responsible for  $NO_x$  generation can be deduced from the emission profiles obtained by the PMT measurements, using interference filters for selecting the  $N_2(C)$  emission at 337 nm, and  $O^*$  emission at 777 nm. The  $N_2(C)$  emission starts with the beginning of both streamer and spark current pulses. During the rising slope of the current pulses, the electrons must have enough energy to ionize, as well

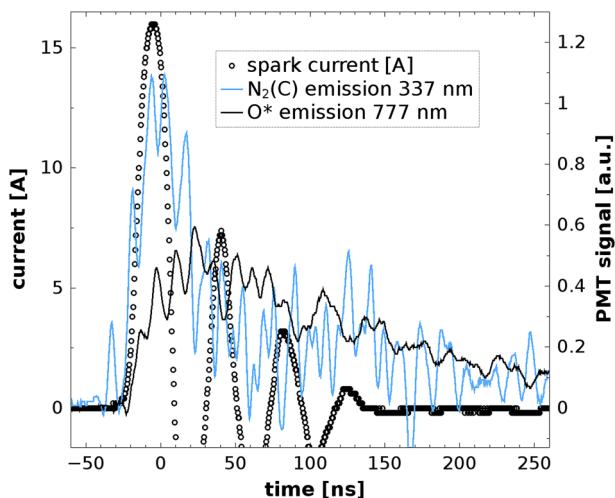


**Fig. 10** Typical PMT signals of the optical emission during the spark phase of TS,  $f \sim 2$  kHz,  $d \approx 6$  mm,  $C \approx 35$  pF,  $R = 9.24$  M $\Omega$ ,  $r = 0$  k $\Omega$

as to excite  $N_2$  molecules. We therefore assume that the majority of the  $N_2(C)$  states are created by high energy electrons:



The fast quenching of excited  $N_2^*$  molecules, such as  $N_2(C)$ , with molecular oxygen is probably one of the major sources of atomic oxygen [54]:



The O atoms may generate NO (Eq. 4), but they can also generate ozone  $O_3$ :



Next, ozone is able to oxidize NO to  $NO_2$ :



These reactions should establish certain equilibrium concentrations of NO,  $NO_2$  and  $O_3$  molecules, depending on the initial concentrations of their precursors, gas temperature and composition. In the streamer corona and other discharges generating atmospheric pressure air plasma with the temperature very close to ambient, the dominant product is ozone, since the reaction (8) is much faster at 300 K than the reaction (4) [51].

In the TS, the streamer is followed by the spark with much higher gas temperature. Ozone generated during the streamer-to-spark transition phase, should be thermally decomposed and the Zeldovich reaction (4) enhanced. In fact, only traces of ozone with concentration below  $\sim 10$  ppm were detected in the outlet gas, according to the obtained infrared spectra (Fig. 11). The negligible amount of  $O_3$  in the gas phase supports our previous findings that nitrites and nitrates generated in the aqueous phase from dissolved NO/ $NO_2$  play crucial role as antimicrobial agent in the water treated by TS, while the role of dissolved  $O_3$  was found negligible [12].

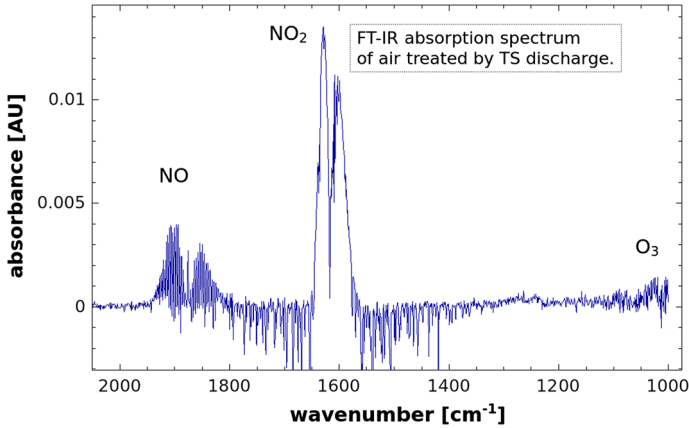
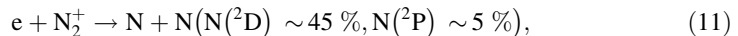
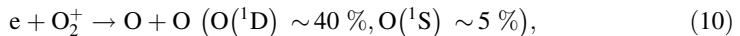


**Fig. 11** Typical FT-IR absorption spectrum of gas treated by TS discharge,  $f \sim 4$  kHz,  $d \approx 6$  mm,  $C \approx 35$  pF,  $R = 9.24$  M $\Omega$ ,  $r = 0$  k $\Omega$

The role of the spark phase of TS is not only thermal decomposition of  $O_3$ . Similarly to the streamer, during the initial phase of the spark with the current rising, the energy of electrons is high enough to ionize, dissociate and excite molecules. The spark phase can therefore strongly influence the overall plasma chemistry, since the electron density during the spark phase ( $n_e > 10^{17}$  cm $^{-3}$  at  $f < 3$  kHz [35]) is much higher than during the streamer phase.

The voltage drop that occurs during the spark phase of the TS (Fig. 2) results in the decrease of the electric field intensity between the electrodes and the decrease of the electron mean energy. The electron temperature  $T_e$  after the spark current pulse decreases to ‘only’  $\sim 10,000$  K [35], so they are unable further to ionize or excite higher electronically excited states of  $N_2$ . However, they can still significantly contribute to the overall O and N atoms generation via dissociative electron–ion recombination reactions:



since the rate coefficients of these reactions are relatively high at  $T_e = 10,000$  K ( $2.3 \times 10^{-8}$  and  $4.6 \times 10^{-8}$  cm $^3$  s $^{-1}$ , respectively [51]), and the total density of positive ions must be approximately as high as the density of electrons. In the next step, the products of the reactions (10) and (11) can enhance the  $NO_x$  synthesis, especially by N production bypassing the rate limiting step in the Zeldovich mechanism (Eq. 4).

The importance of dissociative recombination reactions could also explain higher  $NO_2/NO$  ratio at low TS repetition frequency, where the density of charged particles is the highest. If the dissociative recombination reactions make a significant contribution to the production of atomic oxygen species, there might be enough O to produce not only NO, but also further oxidize it to  $NO_2$  in a three-body reaction (12):



With increasing  $f$  and decreasing degree of ionization in the TS spark phase, the total amount of produced oxygen atoms would decrease. As a result, less NO would be oxidized to  $NO_2$ .

The  $\text{NO}_2/\text{NO}$  ratio could be also decreased at higher TS frequencies due to the growing importance of another NO generation channel. Similarly to the NRP spark discharge [54], we can expect accumulation of atomic oxygen O from the previous TS pulses in the discharge zone at higher repetition frequency. These oxygen atoms can react with excited nitrogen molecules generated during the streamer phase of TS discharge to produce NO:



It was shown recently that this reaction can be an important NO synthesis channel in a nanosecond pulsed discharge [55].

At last, there is another possible mechanism leading to the changes of the  $\text{NO}_2/\text{NO}$  ratio with  $f$  that can additionally contribute. At lower TS frequencies, the temperature right after the streamer is relatively low ( $<400$  K). These conditions should be favorable to the generation of  $\text{O}_3$  (Eq. 8). During the streamer-to-spark transition time, these  $\text{O}_3$  molecules could oxidize a part of the available NO to  $\text{NO}_2$  (Eq. 9). With the increasing  $f$ , the  $T_{str}$  grows and the generation of  $\text{O}_3$  after the streamer is suppressed. As a result, the contribution of ozone to  $\text{NO}_2$  generation becomes negligible. These chemical kinetics considerations can be, however, oversimplified. Further research including kinetic modeling is required to resolve this problem, taking into account more reactions and species.

## Conclusions

Our objective was to investigate the generation of important biocidal agents such as NO,  $\text{NO}_2$  and  $\text{O}_3$ , precursors of RONS in the plasma treated water, by the Transient Spark (TS) discharge in atmospheric pressure air. The TS is a streamer-to-spark transition type discharge initiated by a streamer, with the spark pulse duration and amplitude limited by a small amount of energy stored in the circuit internal capacitance  $C$ . The TS repetition frequency (1–10 kHz) can be controlled by the applied voltage. Similar type of plasma, even at higher pulse repetition frequencies, can be generated using nanosecond repetitive pulsed high voltage power supplies. The advantage of our approach is simpler and cheaper electric setup using DC high voltage power supply.

The TS discharge can be maintained at low energy conditions ( $\sim 1$  mJ/pulse), so that the generated plasma stays out of thermal equilibrium. The non-equilibrium state of plasma generated by TS was confirmed by the optical emission spectroscopic study. Our research confirmed high reactivity of the plasma generated by the TS, and its antimicrobial activity. In dry synthetic air, the TS leads to the formation of  $\text{NO}_x$ : the sum of NO and  $\text{NO}_2$  densities more than 600 ppm was achieved with power input below 6 W ( $\text{NO}_x$  generation rate  $\sim 7 \times 10^{16}$  molecules/J).

The TS characteristics change with the increasing TS repetition frequency. At higher frequencies, the preheating of the gas between the electrodes leads to the decrease of the breakdown voltage, smaller and broader spark pulses, and lower electron density during the spark phase of TS. These changes also influence the induced chemistry and generation of excited O and N atoms and nitrogen oxides. The atomic lines emission intensity and the  $\text{NO}_2/\text{NO}$  ratio decreased with increasing TS repetition frequency.

The excited nitrogen molecules  $\text{N}_2^*$  are produced by excitation by high energy electrons during the rising slope of the current pulses, both streamer and spark. These excited  $\text{N}_2^*$  molecules can lead to the sufficient atomic oxygen production necessary for the synthesis of NO. The spark phase is probably very important for the  $\text{NO}_x$  generation. The

dissociative recombination of  $N_2^+$  and  $O_2^+$  ions with electrons provides additional atomic nitrogen and oxygen for the generation of NO, and oxidation of NO to  $NO_2$ .

Only traces of ozone were detected in the outlet gas, most probably due to its thermal decomposition in the high temperature TS spark phase, as well as due to the oxidation of NO to  $NO_2$  that consumes  $O_3$ . Further research including kinetic modeling and measurement of O species in the ground state is required to prove these hypotheses. In future, we also plan to optimize the  $NO_x$  production by varying parameters of the electric circuit (external resistor, internal capacitance, distance of electrodes).

**Acknowledgments** Effort sponsored by the Slovak Research and Development Agency APVV-0134-12, and Slovak Grant Agency VEGA 1/0918/15.

## References

1. Civitano L (1993) Non-thermal plasma techniques for pollution control (NATO series vol 1). Springer, New York
2. Cernak M, Rahel J, Kovacik D, Simor M, Brablec A, Slavicek P (2004) *Contrib Plasma Phys* 44:492–495
3. Sahni M, Locke BR (2006) *J Hazard Mater* 137:1025–1034
4. Messerle VE, Karpenko EI, Ustimenko AB (2014) *Fuel* 126:294–300
5. Machala Z, Hensel K, Akishev Y (2012) Plasma for bio-decontamination, medicine and food security (NATO science for peace and security series a—chemistry and biology). Springer, Dordrecht
6. Pawlat J (2013) *Eur Phys J Appl Phys* 61:24323
7. Laroussi M, Kong MG, Morfill F, Stolz W (2012) Plasma medicine: applications of low-temperature gas plasmas in medicine and biology. Cambridge University Press, Cambridge
8. Fridman A, Friedman G (2013) Plasma medicine. Wiley, Oxford
9. von Woedtke T, Reuter S, Masur K, Weltmann K-D (2013) *Phys Rep* 530:291–320
10. Graves DB (2012) *J Phys D Appl Phys* 45:263001
11. Machala Z, Chládeková L, Pelach M (2010) *J Phys D Appl Phys* 43:222001
12. Machala Z, Tarabová B, Hensel K, Špetlíková E, Šikurová L, Lukeš P (2013) *Plasma Process Polym* 10:649–659
13. Lukeš P, Doležalová E, Sisrová I, Člupek M (2014) *Plasma Sources Sci Technol* 23:015019
14. Brisset JL, Pawlat J (2015) *Plasma Chem Plasma Proc*. doi:10.1007/s11090-015-9653-6
15. Eliasson B, Hirth M, Kogelschatz U (1987) *J Phys D Appl Phys* 20:1421–1437
16. Gordeyeva EA, Matveyev AA (1994) *Plasma Sources Sci Technol* 3:575–583
17. Knizhnik AA, Potapkin BV, Medvedev DD, Korobtsev SV, Shiryayevskii VL, Rusanov VD (1999) *Tech Phys* 365:336–339
18. Rehbein N, Cooray V (2001) *J Electrostat* 51–52:333–339
19. Rahman M, Cooray V (2003) *Opt Laser Technol* 35:543–546
20. Kim T, Song S, Kim J, Iwasaki R (2010) *Jpn J Appl Phys* 49:126201
21. Rahman M, Vernon C, Montaño R, Liyanage P, Becerr M (2011) *J Electrostat* 69:494–500
22. Shank JL, Silliker JH, Herper RH (1962) *Appl Microbiol* 10:185–189
23. Maricinelli RL, McKay CP (1983) *Appl Environ Microbiol* 46:198–202
24. Carbone P, Benedek K, Ruffo M, Luongo W (2013) Device and method for gas sterilization. US Patent 2013/0230430A1
25. Pavlovich MJ, Ono T, Galleher C, Curtis B, Clark DS, Machala Z, Graves DB (2014) *J Phys D Appl Phys* 47:505202
26. Moiseev T, Misra NN, Patil S, Cullen PJ, Bourke P, Keener KM, Mosnier JP (2014) *Plasma Sources Sci Technol* 23:065033
27. Hao XL, Mattson AM, Edelblute CM, Malik MA, Heller LC, Kolb JF (2014) *Plasma Process Polym* 11:1044–1056
28. Morrow R, Lowke JJ (1997) *J Phys D Appl Phys* 30:614–627
29. Kulikovskiy AA (1998) *IEEE Trans Plasma Sci* 26:1339–1346
30. Loeb LB (1965) Electrical coronas, their basic physical mechanisms. University of California Press, Berkeley
31. Raether H (1964) Electron avalanches and breakdown in gases. Butterworths, London

32. Kobayashi A, Osaki K, Yamabe C (2002) *Vacuum* 65:475–479
33. Bromberg L, Cohn DR, Rabinovich A, Alexeev N (1999) *Int J Hydrogen Energy* 24:1131–1137
34. Kanzawa A (1993) *Plasma Sources Sci Technol* 2:58–62
35. Janda M, Martišoviš V, Hensel K, Dvonč L, Machala Z (2014) *Plasma Sources Sci Technol* 23:065016
36. Janda M, Machala Z, Lacoste DA, Stancu GD, Laux CO (2012) Stabilization of a lean methane-air flame using transient spark discharge. In: Janowski T et al (ed) International symposium on high pressure low temperature plasma chemistry HAKONE XIII (Kazimierz Dolny, Poland, 9–14 September), pp 185–189
37. Walsh JL, Shi JJ, Kong MG (2006) *Appl Phys Lett* 89:161505
38. Pancheshnyi SV, Lacoste DA, Bourdon A, Laux CO (2006) *IEEE Trans Plasma Sci* 34:2478–2487
39. Pai D, Lacoste DA, Laux CO (2008) *IEEE Trans Plasma Sci* 36:974–975
40. Hontanon E, Palomares JM, Stein M, Guo XA, Engeln R, Nirschl H, Kruis FE (2013) *J Nanopart Res* 15:1957
41. Hensel K, Kučerová K, Tarabová B, Janda M, Machala Z, Sano K, Mihai CT, Ciorpac M, Gorgan LD, Jijie R, Pohoata V, Topala I (2015) *Biointerphases* 10:029515
42. Machala Z, Janda M, Hensel K, Jedlovský I, Leštinská L, Foltin V, Martišoviš Morvová M (2007) *J Mol Spectrosc* 243:194–201
43. Janda M, Martišoviš V, Machala Z (2011) *Plasma Sources Sci Technol* 20:035015
44. Janda M, Machala Z, Niklová A, Martišoviš V (2012) *Plasma Sources Sci Technol* 21:045006
45. Gerling T, Hoder T, Brandenburg R, Bussiahn R, Weltmann K-D (2013) *J Phys D Appl Phys* 46:145205
46. Gerling T, Hoder T, Bussiahn R, Brandenburg R, Weltmann K-D (2013) *Plasma Sources Sci Technol* 22:065012
47. Bourdon A, Bonaventura Z, Celestin S (2010) *Plasma Sources Sci Technol* 19:034012
48. Kacem S, Eichwald O, Ducasse O, Renon N, Yousfi M, Charrada K (2012) *J Comput Phys* 231:251–261
49. Barni R, Esena P, Riccardi C (2005) *J Appl Phys* 97:073301
50. Wang Y, DeSilva AV, Goldenbaum GC, Dickerson RR (1998) *J Geophys Res* 103:19149–19159
51. Capitelli M, Ferreira CM, Gordiets BF, Osipov AI (2000) *Plasma kinetics in atmospheric gases*, Springer series on atomic, optical, and plasma physics. Springer, Berlin
52. Herron JT (1999) *J Phys Chem Ref Data* 28:1453–1484
53. Laux CO, Spence TG, Kruger CH, Zare RN (2003) *Plasma Sources Sci Technol* 12:125–138
54. Stancu GD, Kaddouri F, Lacoste DA, Laux CO (2010) *J Phys D Appl Phys* 43:124002
55. Shkurenkov I, Burnette D, Lempert WR, Adamovich IV (2014) *Plasma Sources Sci Technol* 23:065003